Article

Journal of
Nanoscience and Nanotechnology
Vol. 20, 1–7, 2020
www.aspbs.com/jnn

Effect of Synthesis Temperature on the Morphologies, Optical and Electrical Properties of MgO Nanostructures

Suresh Sagadevan[1,*], S. Venilla[2], A. R. Marlinda[1], Mohd. Rafie Johan[1], Yasmin Abdul Wahab[1], Rozalina Zakaria[3], Ahmad Umar[4,5,*], Hosameldin H. Hegazy[6,7], H. Algarni[6], and Naushad Ahmad[8]

[1] *Nanotechnology & Catalysis Research Centre, University of Malaya, Kuala Lumpur-50603, Malaysia*
[2] *PG Research Department of Physics, Jayaraj Annapackiyam College for Women (Autonomous) Periyakulam 625605, Tamilnadu, India*
[3] *Photonics Research Centre, Faculty Science, University of Malaya, Kuala Lumpur-50603, Malaysia*
[4] *Department of Chemistry, Faculty of Science and Arts, Najran University, Najran 11001, Saudi Arabia*
[5] *Promising Centre for Sensors and Electronic Devices (PCSED), Najran University, Najran 11001, Saudi Arabia*
[6] *Department of Physics, Faculty of Science, King Khalid University, Abha-61421, Saudi Arabia*
[7] *Department of Physics, Faculty of Science, Al-Azhar University, Assiut 71524, Egypt*
[8] *Department of Chemistry, College of Science, King Saud University, Riyadh-11451, Kingdom of Saudi Arabia*

Herein, we report the effect of synthesis temperature on the morphologies, optical and electronic properties of magnesium oxide (MgO) nanostructures. The MgO nanostructures were synthesized at different temperatures, i.e., 100 °C, 300 °C, and 600 °C by simple chemical reaction process and their morphology, particle size, optical, and electrical properties were examined by different techniques such as scanning electron microscopy (SEM), X-ray diffraction (XRD), Fourier transform infrared (FTIR) spectroscopy and UV-Vis. spectroscopy. The morphological investigations revealed that various morphologies of MgO nanostructures, i.e., nanoparticles, nanosheet networks, and nanoneedles were synthesized at 100 °C, 300 °C, and 600 °C. The XRD results confirmed that with increasing the synthesis temperature, the crystallinity of the synthesized nanostructures increases. Further, the dielectric properties and AC conductivity at various frequencies for MgO nanostructures were studied which revealed that the dielectric losses decrease with increase in frequency and temperature. In addition, the observed band gap decreases from 4.89 eV to 4.438 eV (100 °C to 600 °C) representing its increase in the conductivity.

Keywords: MgO, Nanostructures, Morphology, Optical and Electrical Properties.

1. INTRODUCTION

Magnesium oxide (MgO) is one the most fascinating and promising materials with remarkable electronic, optical, magnetic, thermodynamic, mechanical and electric properties in the metal oxide family [1–3]. Because of its unique structural characteristics, MgO possess various unique characteristics such as non-toxic insulation, wide band gap, simple stoichiometry, low dielectric constant (9×10^{-3}), low thermal conductivity (42 $Wm^{-1}K^{-1}$ at 275 K), high ionic properties, biocompatibility, low refractive index (1.74), simple crystal structure and so on [4–8]. Due to its biocompatibility, MgO is also used for various bio-applications such as antibacterial and anticancer agents, biosensors, reactive oxygen species (ROS), bone regeneration and so forth [9–13]. The interesting properties of MgO enabled it to be efficiently used for variety of high-technological applications, to name a few, adsorption, electronics, reflecting and anti-reflecting coatings, fire retardants, ceramics, catalysis, petrochemicals, chemical and toxic waste management, detection and remediation, light emitting diodes (LEDs), solar cells, laser diodes and many more [14–21]. Therefore, because of remarkable properties and wide applications, various MgO nanomaterials such as nanowires, nanobelts, nanotubes, fishbone shaped structures, nanocrystals, nanoparticles, nanofibers, nanoflakes, nano and microspheres, *grass-like*, and so on were synthesized by several techniques and reported in the literature [22–29]. Karthik et al. demonstrated the synthesis of MgO nanostructures by microwave assisted hydrothermal method and

*Authors to whom correspondence should be addressed.

examined their utilization for environmental remediation, antibacterial and anticancer applications [9]. Mesoporous MgO nanostructures were synthesized by *the* surfactant template process for enhanced adsorption and antimicrobial activity and reported in the literature [10]. Darvishi et al. reported the sonochemical synthesis of MgO nanostructures and used it for decolorization of synthetic textile *wastewater* [24]. Applying sol–gel combustion synthesis using different fuels, Nassar et al. demonstrated the synthesis of MgO nanostructures for their efficient application as nano-adsorbent for the removal of reactive red 195 and orange G [26]. Using an interfacial reaction in a solid-stabilized emulsion method, MgO nano and microspheres were synthesized and reported in the literature [29].

In this paper, we report the facile synthesis of MgO nanostructures by *a* simple chemical reaction process based on different synthesis temperatures. The synthesized MgO nanostructures were systematically characterized in terms of their morphological, structural, optical and electrical properties.

2. EXPERIMENTAL DETAILS

2.1. Synthesis of MgO Nanostructures

For the synthesis of MgO nanostructures, all the materials were analytical grade and used as received without any purification. To synthesize the MgO nanomaterials, magnesium acetate ($Mg(CH_3COO)_2$, Sigma-Aldrich), sodium hydroxide anhydrous pellets (NaOH, Sigma-Aldrich) and polyvinyl alcohol (PVA, Sigma-Aldrich) were used. Deionized (DI) water was used as *a* solvent to synthesize all nanomaterials. In a typical reaction process, *an* aqueous solution of NaOH (0.5 M, 50 mL) was added dropwise into the aqueous solution of $Mg(CH_3COO)$ (0.1 M, 50 mL) under constant stirring. Consequently, 0.1 M PVA solution was added in the resultant solution and stirred the solution for 1 hr. The pH = 9.0 was *maintained* for the solution. The obtained reaction mixture was subjected to refluxing for 6 hrs at different reaction temperatures, i.e., 100 °C, 300 °C, and 600 °C. The obtained precipitate was decanted and washed with DI water and ethanol sequentially, and dried at 90 °C for 2 hrs. Finally, all the synthesized materials were calcined to 700 °C for 4 hrs which resulted *in* the formation of pure MgO nanostructures.

2.2. Characterizations of MgO Nanostructures

The phase purity of synthesized MgO nanostructures were characterized by X-ray diffraction (XRD; Philips X'pert Pro diffractometer) measured with Cu-Kα radiation (λ = 1.5406 Å) in 2θ range of 10–80°. The morphologies of the synthesized materials were examined by scanning electron microscopy (SEM, Carl Zeiss MA15/EVO 18) while the chemical composition was studied by Fourier transform infrared (FTIR; Perkin Elmer) spectroscopy. The optical properties were characterized by UV-Visible spectroscopy (UV-vis Schimadzu 1800 spectrophotometer) in the range of 200–700 nm at room temperature. The dielectric properties of the synthesized nanostructures were examined in the frequency range of 50 Hz–5 MHz by LCR meter (HIOKI 3532-50 LCR HITESTER).

3. RESULTS AND DISCUSSION

3.1. Structural, Morphological and Compositional Properties of MgO Nanostructures

Figure 1 exhibits the typical XRD patterns of MgO nanostructures synthesized at different temperatures, i.e., 100 °C, 300 °C, and 600 °C. It is interesting to note that all the observed diffraction peaks are well-matched with the characteristic peaks of pure cubic phase MgO [29]. The observed diffraction patterns correspond to the crystal planes of MgO (111), (200), (220) and (311), respectively. The observed diffraction patterns are well matched with the reported literature and JCPDS card no. 4-829 [28]. Except *for* MgO, no other diffraction peaks are observed in the pattern which confirmed that the synthesized materials are pure MgO without any significant impurity. In addition, all the peaks are sharp and strong which revealed the well-crystallinity of the synthesized MgO nanostructures.

The crystallite size of the prepared MgO nanostructures were examined by Debye-Scherrer's equation as mentioned below:

$$D = 0.9\lambda/\beta\cos\theta$$

Where D is the crystallite size, λ is the wavelength of the X-ray beam, β is the FWHM-full width at half maximum of the most intense peak and 2θ is the Bragg diffraction angle of the most intense peak. The calculated crystallite size of the synthesized MgO nanostructures at 100 °C, 300 °C, 600 °C were 9, 11 and 15 nm, respectively. The observed XRD results revealed that the grain sizes of the synthesized MgO nanostructures were increased with increasing the synthesis temperature, most probably because of the agglomeration process induced from thermal annealing due to electrostatic forces.

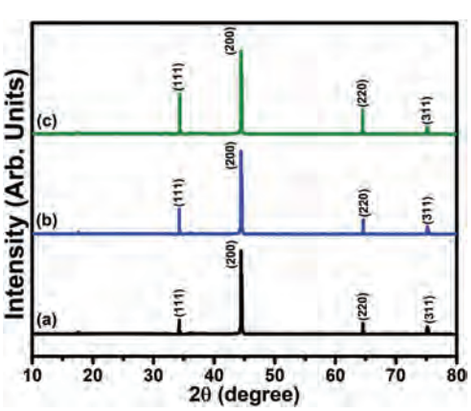

Figure 1. Typical XRD pattern of synthesized MgO nanostructures at different temperatures; (a) 100 °C (b) 300 °C and (c) 600 °C.

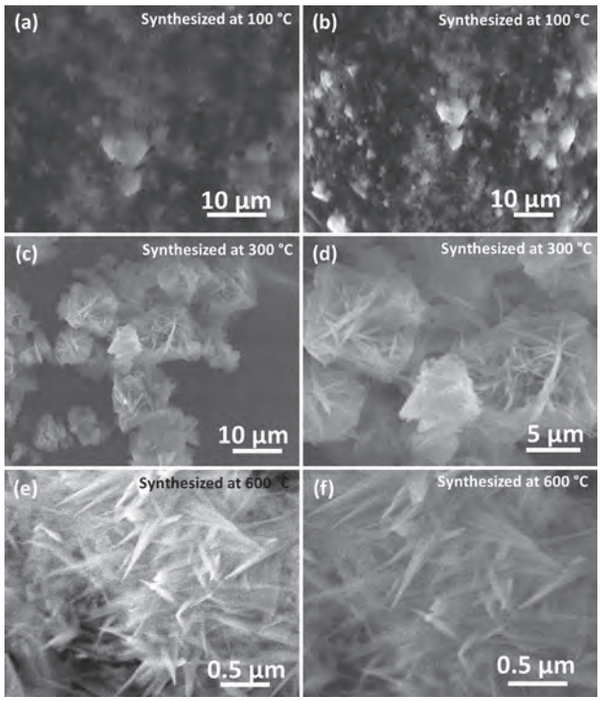

Figure 2. Typical SEM images of synthesized MgO nanostructures at different temperatures; (a and b) 100 °C (c and d) 300 °C and (e and f) 600 °C.

The general morphologies of the synthesized MgO nanostructures were examined by scanning electron microscopy (SEM). Figure 2 exhibits the typical SEM images of the synthesized MgO nanostructures synthesized at different temperatures, i.e., 100 °C, 300 °C and 600 °C. Figures 2(a) and (b) exhibit the typical SEM images of the MgO material synthesized at 100 °C which revealed the high-density growth of spherical shaped particles. The synthesized particles are in nano-dimension thus termed as, "nanoparticles." The nanoparticles are grown in very high density thus much agglomeration is seen in the observed micrographs. The typical sizes of the synthesized nanoparticles are in the range of 100 ± 30 nm.

Interestingly, when the synthesis temperature was increased to 300 °C, the morphologies of the synthesized MgO material was changed to sheet-like structures (Figs. 2(c and d)). These sheets like morphologies are grown in high density and arranged in a specific flower-shaped *structures*. Due to high-density growth, the grown sheets are intermingled in each other and form the interconnects in the flower-shaped structures. The typical thickness of the nanosheets are 120 ± 30 nm while the size of the full flower-shaped structure was in the range of 8–10 μm. Interestingly, upon increasing the synthesis reaction temperature to 600 °C, MgO nanoneedles were formed which are grown in high density (Figs. 2(e and f)). The synthesized nanoneedles exhibited sharp tips with wider bases. The typical sizes of the nanoneedles at their tips are 25 ± 5 nm and lengths are 500 ± 50 nm.

The chemical compositions of the synthesized MgO nanostructures were characterized by FTIR spectroscopy. Figure 3 exhibits the typical FTIR spectra recorded in the range of 500 cm^{-1} to 4000 cm^{-1}. The observed FTIR spectra show various well-defined peaks appeared at 3443 cm^{-1}, 3158 cm^{-1}, 1643 cm^{-1}, 1409 cm^{-1}, 1118 cm^{-1}, 870 cm^{-1}, 613 cm^{-1} and 517 cm^{-1}. The broad peaks appeared at 1643 cm^{-1} and 3158–3443 cm^{-1} were related to the bending and stretching frequencies of the hydroxyl group, respectively [30]. The peak appeared at 613 cm^{-1} correspond to the Mg–O [31, 32]. The peaks at 517 cm^{-1} and 870 cm^{-1} revealed the existence of stretching and bending vibration modes of Mg–O bond, respectively [32].

3.2. Optical Properties of MgO Nanostructures

The optical properties of the synthesized MgO nanostructures were examined by UV-Visible spectroscopy. Figure 4 exhibits the typical UV-Visible spectra of synthesized MgO nanostructures in the wavelength range between 200–700 nm. The UV absorption edge shows a single peak appeared at around ~255, ~265 and ~280 nm for the MgO nanostructures synthesized at 100 °C, 300 °C, and 600 °C, respectively. The broad peak appeared at 280 nm in the MgO nanoneedles synthesized at 600 °C shows that the UV absorption edge possesses quantum confinement [33]. It was observed that at first, the absorbance decreases sharply with the increase in wavelength, near the edge of the band indicating the sample possess nanostructure [34], thereafter the absorption coefficient value was constant indicating the size uniformity of the MgO nanostructures.

The band gap for the synthesized MgO nanostructures was estimated using the Tauc plot. Figure 5 shows the plot of $(\alpha h\upsilon)^2$ versus $h\upsilon$ for the MgO nanostructures. From the

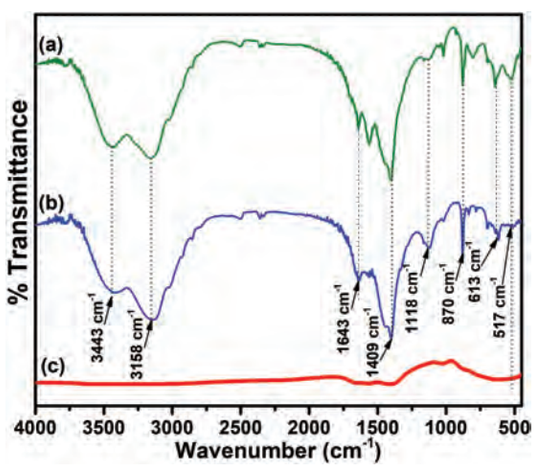

Figure 3. Typical FTIR spectra of synthesized MgO nanostructures at different temperatures; (a) 100 °C (b) 300 °C and (c) 600 °C.

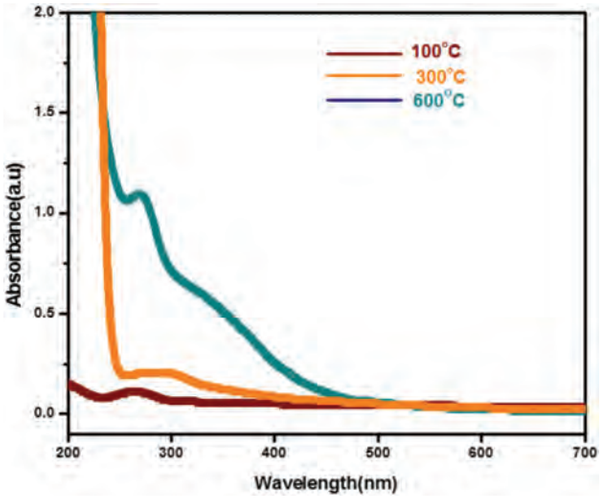

Figure 4. Typical UV-visible spectra of synthesized MgO nanostructures at different temperatures; 100 °C, 300 °C, and 600 °C.

plot, the band gap values of the MgO nanostructures were calculated to be 4.89 eV, 4.84 eV, 4.43 eV for the samples synthesized at 100 °C, 300 °C, and 600 °C, respectively. With increasing synthesis temperature, the band gap values of MgO NS decrease gradually. In addition, with increasing synthesis temperature, the decrease in band gap should be associated with increased grain size, decreased carrier concentration, tensile stress and oxygen vacancies leading to decreased carrier concentration in the conductive band [35]. Annealing process, on the other hand, improves crystallinity, increases the average grain size and decreases defects [35].

3.3. Electrical Properties of MgO Nanostructures

The dielectric constant was measured as a function of the frequency at room temperatures for MgO nanostructures

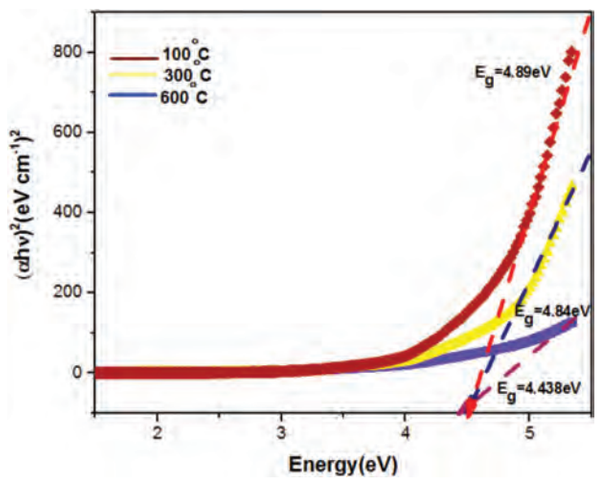

Figure 5. The calculated band gaps of the synthesized MgO nanostructures at different temperatures; 100 °C, 300 °C, and 600 °C.

synthesized at different temperatures, i.e., 100 °C, 300 °C and 600 °C (Fig. 6). The corresponding dielectric losses are depicted in Figures 6(A) and (B) which shows a plot of dielectric constant versus applied frequency. It is observed in Figure 6(A) that with increasing frequency, the dielectric constant decreases exponentially and attains a constant value in the high-frequency region [36]. This refers to decreasing polarization of the space charge in relation to total polarization. The ionic polarization slightly interacts with the field of frequency variation associated with electronic polarization; this is because of an ion's mass is superior to the electron. The electrons react even to the high frequencies in the field of vibrations [37]. The dielectric constant increases with the synthesized MgO nanoneedles synthesized at 600 °C, which carries numbers due to the increase in the charge. The improvement in low-frequency dielectric constant is a function of orientation and interfacial polarization and is due to the presence of defects [38]. This is because, at lower frequencies, the strong interfacial polarization caused the accumulation of charge carrier boundaries of MgO nanostructures in respect to the field applied as it allows the charge carrier to have enough time to be collected at the conductive boundary as well as to enhance the dielectric constant value [39]. As the frequency increases, the polarization starts to decrease and drops to a constant value due to relaxation [40]. Figure 6(B) shows the dielectric loss as a function of the frequency for MgO nanostructures synthesized at different temperatures. It is found that the dielectric loss decreases with increase in frequency and temperature, which can be accounted for due to a decrease in the contribution of space charge polarization with frequency [41]. High energy loss is observed in the low-frequency region, which may be due to low-frequency dielectric polarization, space-charge and electron movement in rotational fashion [42].

Figure 6(C) shows the variation of A.C electrical conductivity as a function of frequency for MgO nanostructures. As seen in the figure, with the increase in frequency, the A.C electrical conductivity is increased, this is due to the polarization of the space charge. We noticed miserable semi-circles for MgO nanostructures as shown in Figure 6(D). Complex impedance diagrams reflecting the variation of the imaginary part a function of the real part show that the experimental points are located on circle arcs that do not pass through the origin and are centered below the real axis. This semi-circular curve asymmetry indicates a deviation from the ideal Debye type behavior and can be explained by non-Debye relaxation behavior [43]. This means that in the frequency range applied, MgO follows non-Debye relaxation behavior. The primary causes of non-ideal behavior are the nature of grain size distribution, defects, inhomogeneity and grain boundary effect in the material [44].

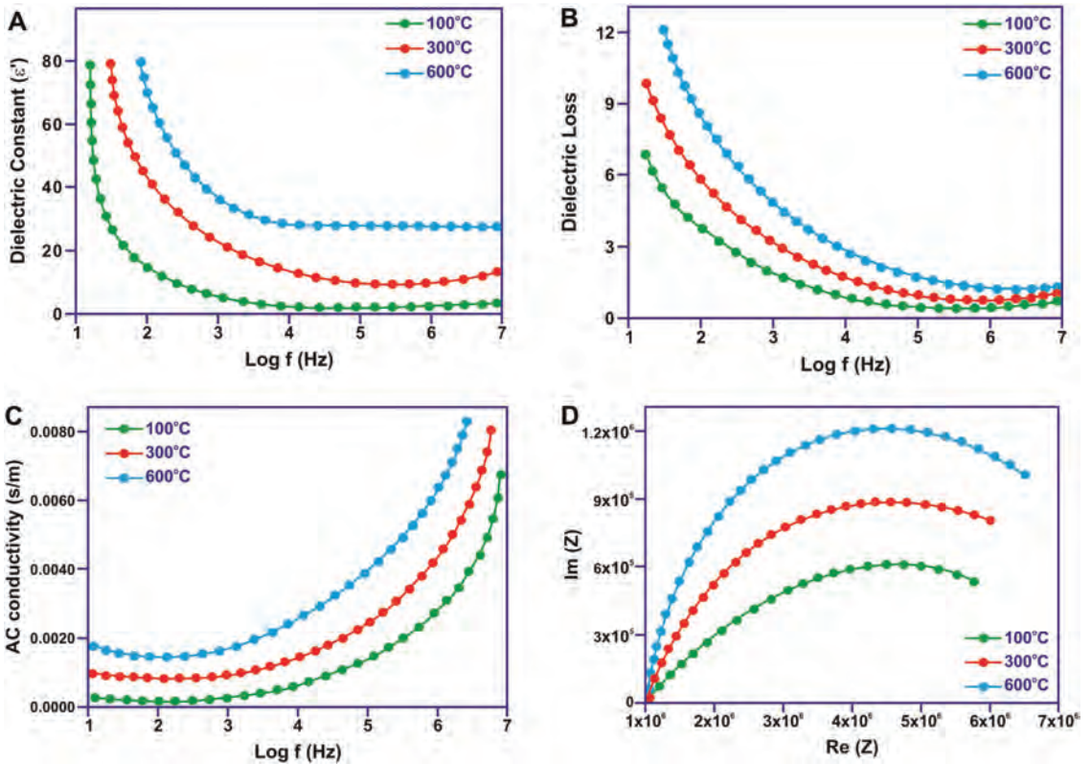

Figure 6. (A) Dielectric constant (B) dielectric loss (C) AC conductivity of MgO NS for variation with different frequencies (D) impedance spectrum of MgO NS.

4. CONCLUSION

In summary, temperature-dependent synthesis of MgO nanostructures was done by facile chemical reaction process. Several MgO nanostructures, such as nanoparticles, nanosheets composed in flower-shaped structures and nanoneedles were synthesized at various synthesis temperatures, i.e., 100 °C, 300 °C, and 600 °C, respectively. The calculated grain sizes for the MgO nanostructures at 100 °C, 300 °C and 600 °C were 9, 11, 15 nm, respectively. It was observed that the absorbance decreases sharply with an increase in wavelength near the band edge indicating the formation of *the* nanostructure. The calculated band gaps were 4.89 eV, 4.84 eV and 4.43 eV for the MgO nanostructures synthesized at 100 °C, 300 °C and 600 °C, respectively. The observed electrical properties show that the dielectric constant and dielectric loss of the MgO nanostructures decreases as the frequency increases. Moreover, the A.C electrical conductivity increases with the increase of frequency. The impedance analysis of MgO nanostructures confirmed relaxation in the non-Debye type relaxation in the applied frequency range.

Acknowledgments: One of the authors (Suresh Sagadevan) acknowledges the honor, namely the "Senior Research Fellow" at Nanotechnology and Catalysis Research Centre (NANOCAT), University of Malaya, Malaysia. The authors gratefully thank the Deanship of Scientific Research at King Khalid University for the financial support through research groups program under grant number (R.G.P.2/18/40).

References and Notes

1. Utamapanya, S., Klabunde, K.J. and Schlup, J.R., **1991**. Nanoscale metal oxide particles/clusters as chemical reagents. Synthesis and properties of ultrahigh surface area magnesium hydroxide and magnesium oxide. *Chemistry of Materials, 3*(1), pp.175–81.
2. Rajagopalan, S., Koper, S., Decker, S. and Klabunde, K.J., **2002**. Nanocrystalline metal oxides as destructive adsorbents for organophosphorus compounds at ambient temperatures. *Chemistry: A European Journal, 8*(11), pp.2602–2607.
3. Sing, J.P., Lim, W.C., Lee, I.J., Won, S.O. and Chae, K.H., **2018**. Surface structure of MgO thin films revealed from X-ray reflectivity and near-edge X-ray absorption fine structure measurements. *Science of Advanced Materials, 10*, pp.1372–1376.
4. El-Gharkawy, El-Sayed, R.H. and Ammar, H.Y., **2018**. Adsorption of CO on TM-deposited $(MgO)_{12}$ nano-cage (TM = Ni, Pd, and Pt): A study on electronic properties. *Journal of Nanoelectronics and Optoelectronics, 13*, pp.546–553.
5. Li, X., Pu, Y., Zhu, X., Dong, Z., Tian, Y. and Zhang, L., **2018**. The broaden dielectric temperature stability of $Bi(Mg_{0.5}Zr_{0.5})O_3$ doped on $BaTiO_3$ based ceramics. *Science of Advanced Materials, 10*, pp.248–252.
6. Xu, B.Q., Wei, J.H., Wang, H.Y., Sun, K.Q. and Zhu, Q.M., **2001**. Nano-MgO: Novel preparation and application as support of Ni catalyst for CO_2 reforming of methane. *Catalysis Today, 68*(1–3), pp.217–225.

7. Wang, C., Guo, T., Sun, M., Li, C., Guo, M., Li, C. and Wang, Q., **2018**. Transesterification of dimethyl carbonate with phenol to diphenyl carbonate over magnesium oxide nanosheets. *Science of Advanced Materials, 10*, pp.779–784.
8. Tang, H., Chen, K., Li, X., Ao, M., Guo, X. and Xue, D., **2018**. Advanced flame retardant magnesium-based materials: System optimization toward enhanced performance of thermoplastic elastomer. *Science of Advanced Materials, 10*, pp.1431–1437.
9. Karthik, K., Dhanuskodi, S., Gobinath, C., Prabukumar, S. and Sivaramakrishnan, S., **2019**. Fabrication of MgO nanostructures and its efficient photocatalytic, antibacterial and anticancer performance. *Journal of Photochemistry and Photobiology B: Biology, 190*, pp.8–20.
10. Sharma, J., Sharma, M. and Basu, S., **2017**. Synthesis of mesoporous MgO nanostructures using mixed surfactants template for enhanced adsorption and antimicrobial activity. *Journal of Environmental Chemical Engineering, 5*(4), pp.3429–3438.
11. Umar, A., Rahman, M.M. and Hahn, Y.B., **2009**. MgO polyhedral nanocages and nanocrystals based glucose biosensor. *Electrochemistry Communications, 11*, pp.1355–1357.
12. Zhang, K., An, Y., Zhang, L. and Dong, Q., **2012**. Preparation of controlled nano-MgO and investigation of its bactericidal properties. *Chemosphere, 89*, pp.1414–1418.
13. Zaki, H.M., Al-Heniti, S., Ahmad Umar, F., Al-Marzouki, A., Abdel-Daiem, T.A., Elmosalami, H.A., Dawoud, F.S., Al-Hazmi, S.S. and Ata-Allah, **2013**. Magnesium-zinc ferrite nanoparticles: Effect of copper doping on the structural, electrical and magnetic properties. *Journal of Nanoscience and Nanotechnology, 13*, pp.4056–4065.
14. Umar, A., Al-Hazmi, F., Dar, G. N., Zaidi, S.A.M., Al-Tuwirqi, R., Alnowaiser, F., Al-Ghamdi, A.A. and Hwang, S.W., **2012**. Ultrasensitive ethanol sensor based on rapidly synthesized $Mg(OH)_2$ hexagonal nanodisks. *Sensors and Actuators B: Chemical, 166–167*, pp.97–102.
15. Al-Hazmi, F., Umar, A., Dar, G.N., Al-Ghamdi, A.A., Al-Sayari, S.A., Al-Hajry, A., Kim, S.H., Al-Tuwirqi, R.M., Alnowaiser, F. and El-Tantawy, F., **2012**. Microwave-assisted rapid growth of $Mg(OH)_2$ nanosheet networks for ethanol chemical sensor application. *Journal of Alloys and Compounds, 519*, pp.4–8.
16. Salem, A.N.M., Ahmed, M.A. and El-Shahat, M.F., **2016**. Selective adsorption of amaranth dye on Fe_3O_4/MgO nanoparticles. *Journal of Molecular Liquids, 219*; pp.780–788.
17. Aly, H.M., Moustafa, M.E., Nassar, M.Y. and Abdelrahman, E.A., **2015**. Synthesis and characterization of novel Cu(II) complexes with 3-substituted-4-amino-5-mercapto-1,2,4-triazole Schiff bases: A new route to CuO nanoparticles. *Journal of Molecular Structures, 1086*, pp.223–231.
18. Swaroop, C. and Shukla, M., **2018**. Nano-magnesium oxide reinforced polylactic acid biofilms for food packaging applications. *International Journal of Biological Macromolecules, 113*, pp.729–736.
19. Krishnamoorthy, K., Jeong, Y.M., Ho, B.H., Somi, K.C. and Kim, S.J., **2012**. Mechanistic investigation on the toxicity of MgO nanoparticles toward cancer cells. *Journal of Materials Chemistry, 22*, pp.24610–24617.
20. Bagheri, G.H., Sabbaghan, M. and Mirgani, Z., **2015**. A comparative study on properties of synthesized MgO with different templates. *Spectrochimica Acta Part A: Molecular and Biomolecular Spectroscopy, 137*, pp.1286–91.
21. Li, H., Li, M., Wang, X., Wu, X., Liu, F. and Yang, B., **2013**. Synthesis and optical properties of single-crystal MgO nanobelts. *Materials Letters, 102–103*, pp.80–82.
22. Al-Gaashani, R., Radiman, S., Al-Douri, Y., Tabet, N. and Daud, A.R., **2012**. Investigation of the optical properties of $Mg(OH)_2$ and MgO nanostructures obtained by microwave-assisted methods. *Journal of Alloys and Compounds, 521*(25), pp.71–76.
23. Zhao, M., Chen, X.L., Zhang, X.N., Li, H., Li, H.Q. and Wu, L., **2004**. Preparation and characterization of networked rectangular MgO nanostructures. *Chemical Physics Letters, 388*(1–3), pp.7–11.
24. Soltani, R.D.C., Safari, M. and Mashayekhi, M., **2016**. Sonocatalyzed decolorization of synthetic textile wastewater using sonochemically synthesized MgO nanostructures. *Ultrasonics Sonochemistry, 30*, pp.123–131.
25. Smovzh, D.V., Sakhapov, S.Z., Zaikovskii, A.V., Chernova, S.A. and Novopashin, S.A., **2019**. Formation mechanism of MgO hollow nanospheres via calcination of C-MgO composite produced by electric arc spraying. *Ceramics International, 456*(6), pp.7338–7343.
26. Nassar, M.Y., Mohamed, T.Y., Ahmed, I.S. and Samir, I., **2017**. MgO nanostructures via a sol–gel combustion synthesis method using different fuels: An efficient nano-adsorbent for the removal of some anionic textile dyes. *Journal of Molecular Liquids, 225*, pp.730–740.
27. Yang, Q., Sha, J., Wang, L., Wang, J. and Yang, D., **2006**. MgO nanostructures synthesized by thermal evaporation. *Materials Science and Engineering: C, 26*(5–7), pp.1097–1101.
28. Nusheh, M., Yoozbashizadeh, H., Askari, M., Kobatake, H. and Fukuyama, H., **2010**. Mechanically activated synthesis of single crystalline MgO nanostructures. *Journal of Alloys and Compounds, 506*(2), pp.715–720.
29. He, Y., **2006**. MgO nanostructures microspheres synthesized by an interfacial reaction in a solid-stabilized emulsion. *Materials Letters, 29*(29–30), pp.3511–3513.
30. Nagappa, B. and Chandrappa, G.T., **2007**. Mesoporous nanocrystalline magnesium oxide for environmental remediation. *Microporous and Mesoporous Materials, 106*(1–3), pp.212–218.
31. Mirzaei, H. and Davoodnia, A., **2012**. Microwave-assisted sol–gel synthesis of MgO nanoparticles and their catalytic activity in the synthesis of hantzsch 1,4-dihydropyridines. *Chinese Journal of Catalysis, 33*(9–10), pp.1502–1507.
32. Kumar, D., Yadav, L.S.R., Lingaraju, K., Manjunath, K., Suresh, D., Prasad, D., Nagabhushana, H., Sharma, S.C., Naika, H.R., Chikkahanumantharayappa and Nagaraju, G. **2015.** Combustion synthesis of MgO nanoparticles using plant extract: Structural characterization and photoluminescence studies. *AIP Conference Proceedings*, *1665*, pp.050145–3.
33. Sagadevan, S. and Podder, J., **2015**. Investigations on structural, optical, morphological and electrical properties of nickel oxide nanoparticles. *International Journal of Nanoparticles, 8*(3–4), pp.289–301.
34. Bhaiswar, J.B., Salunkhe, M.Y. and Dongre, S.P., **2013**. Synthesis, characterization, thermal stability and D.C. electrical conductivity of Pani/Pbs nanocomposite. *International Journal of Composite Materials, 3*, pp.115–121.
35. Caglar, M., Ilican, S., Caglar, Y. and Yakuphanoglu, F., **2009**. Electrical conductivity and optical properties of ZnO nanostructured thin film. *Applied Surface Science, 255*, pp.4491–4496.
36. Sagadevan, S., Johan, M.R.B., Aziz, F.A., Hsu, H.L. Selvin, R., Hegazy, H.H., Umar, A., Algarni, H. and Selva R.L., **2019**. Nickel doped tin oxide nanoparticles: Magnetic, dielectric, and electrical properties. *Journal of Nanoelectronics and Optoelectronics, 14*, pp.614–621.
37. Sagadevan, S., Podder, J. and Das, I., **2016**. Hydrothermal synthesis of zirconium oxide nanoparticles and its characterization. *Journal of Materials Science: Materials in Electronics, 27*, pp.5622–5627.
38. Selvi, K.T., Alamelumangai, K., Priya, M., Rathnakumari, M., Kumar, P.S. and Sagadevan, S., **2016**. Studies on electrical properties of MgO/Pr_6O_{11} nanocomposite. *Nanomaterials and Nanotechnology, 6*, pp.1–5.
39. Sagadevan, S. and Priya, M., **2015**. Electrical properties of copper oxide nanoparticles. *Journal of Nano Research, 30*, pp.1–8.
40. Vijayamari, A., Sadayandi, K., Sagadevan, S. and Singh, P., **2017**. A study of optical, surface morphological and electrical properties of manganese oxide nanoparticles. *Journal of Materials Science: Materials in Electronics, 28*, pp.2739–2746.

41. Mangai, K.A., Selvi, T., Priya, M., Rathnakumari, M., Sureshkumar, P. and Sagadevan, S., **2017**. Investigations on dielectric and impedance properties of M-type hexaferrite. *Journal of Materials Science: Materials in Electronics, 28*(3), pp.2910–2922.

42. Sagadevan, S., Chowdhury, Z.Z., Johan, M.R.B., Aziz, F.A., Roselin, S.L., Podder, J., Letter, A. and Selvin, R., **2019**. Cu-doped SnO_2 nanoparticles: Synthesis and properties. *Journal of Nanoscience and Nanotechnology, 19*, pp.7139–7148.

43. Das, R. and Choudhary, R.N.P., **2018**. Studies of structural, dielectric relaxation and impedance spectroscopy of lead-free double perovskite: Dy_2NiMnO_6. *Journal of Materials Science: Materials in Electronics, 29*, pp.19099–19110.

44. Al-Zangana, S., Iliut, M., Boran, G., Turner, M., Vijayaraghavan, A. and Dierking, I., **2016**. Dielectric spectroscopy of isotropic liquids and liquid crystal phases with dispersed graphene oxide. *Scientific Reports, 6*, p.31885.

Received: 12 January 2019. Accepted: 15 April 2019.